Initialization of the HIRLAM Model Using a Digital Filter

PETER LYNCH AND XIANG-YU HUANG

Department of Meteorology, Stockholm University, Stockholm, Sweden

(Manuscript received 10 June 1991, in final form 27 August 1991)

ABSTRACT

Spurious high-frequency oscillations occur in forecasts made with the primitive equations if the initial fields of mass and wind are not in an appropriate state of balance with each other. These oscillations are due to gravity–inertia waves of unrealistically large amplitude; the primary purpose of initialization is the removal or reduction of this high-frequency noise by a delicate adjustment of the analyzed data. In this paper a simple method of eliminating spurious oscillations is presented. The method uses a digital filter applied to time series of the model variables generated by short-range forward and backward integrations from the initial time.

The digital filtering technique is applied to initialize data for the High-Resolution Limited-Area Model (HIRLAM). The method is shown to have the three characteristics essential to any satisfactory initialization scheme: (i) high-frequency noise is effectively removed from the forecast; (ii) changes made to the analyzed fields are acceptably small; (iii) the forecast is not degraded by application of the initialization.

The digital filtering initialization (DFI) technique is compared to the standard nonlinear normal-mode initialization (NMI) used with the HIRLAM model. Both methods yield comparable results, though the filtering appears more effective in suppressing noise in the early forecast hours. The computation time required for initialization is about the same for DFI and NMI. The outstanding appeal of the digital filtering technique is its great simplicity in conception and application.

1. Introduction

A simple initialization method based on the concept of digital filters is described in this report. The theoretical basis of the scheme is presented, and an application to a sophisticated baroclinic limited-area model shows that the method is very effective in eliminating spurious high-frequency oscillations from the forecast.

The implementation of the digital filtering technique is extremely simple. Two short-range adiabatic integrations of the forecast model are carried out from the initial data, one forward and one backward in time, each being typically for a duration of 3 h. The prognostic variables at each grid point are multiplied by a weight that varies with time, and the totals for the two integrations are added to yield the filtered initial conditions. The weights, given by a simple analytical expression, are chosen to bring about the desired filtering of the data.

The digital filtering initialization (DFI) scheme was compared to the standard initialization scheme used with the High-Resolution Limited-Area Model (HIRLAM) (Källberg 1989). The HIRLAM model is the forecast component of a comprehensive numerical weather prediction system under development in a joint Nordic–Dutch–Irish research project.

Corresponding author address: Dr. Peter Lynch, Meteorological Service, Glasnevin Hill, Dublin 9, Ireland.

The reference initialization method is a particular formulation of the nonlinear normal-mode initialization (NMI) technique using the criterion, proposed by Machenhauer (1977), that the initial tendencies of the gravity waves be set to zero. Several measures of the efficacy of the digital filtering and normal-mode initialization schemes in removing gravity–inertia-wave oscillations from the forecast were investigated. In the particular case study described in this report, the digital filtering technique was more effective in suppressing high-frequency noise. Computation time was comparable for the two methods, but there is considerable scope for reduction in the case of DFI, by more careful design of the filter.

2. Theoretical framework

A general discussion of filtering, from the perspective of geophysics, can be found in Båth (1974). More specific information on digital filters, with references to the literature on signal processing, is given in Hamming (1989).

a. Filtering a continuous function

Consider a function of time $f(t)$ with low- and high-frequency components. To filter out the high frequencies one may proceed as follows:

1) calculate the Fourier transform $F(\omega)$ of $f(t)$;
2) set the coefficients of the high frequencies to zero;
3) calculate the inverse transform.

Step 2 may be performed by multiplying $F(\omega)$ by an appropriate weighting function $H(\omega)$. Typically, $H(\omega)$ is a step function

$$H(\omega) = \begin{cases} 1, & |\omega| \leq |\omega_c|; \\ 0, & |\omega| > |\omega_c|, \end{cases} \tag{1}$$

where ω_c is a cutoff frequency. These three steps are equivalent to a convolution of $f(t)$ with $h(t) = \sin(\omega_c t)/\pi t$, the inverse Fourier transform of $H(\omega)$. This follows from the convolution theorem

$$\mathcal{F}\{(h*f)(t)\} = \mathcal{F}\{h\} \cdot \mathcal{F}\{f\} = H(\omega) \cdot F(\omega) \tag{2}$$

(see Fig. 1). Thus, to filter $f(t)$ one calculates

$$f^*(t) = (h*f)(t) = \int_{-\infty}^{+\infty} h(\tau) f(t-\tau) d\tau. \tag{3}$$

For simple functions $f(t)$, this integral may be evaluated analytically. In general, some method of approximation must be used.

b. *Filtering a discrete function*

Suppose now that f is known only at discrete moments $t_n = n\Delta t$, so that the sequence $\{\ldots, f_{-2}, f_{-1}, f_0, f_1, f_2, \ldots\}$ is given. For example, f_n could be the value of some model variable at a particular grid point at time t_n. The shortest period component that can be represented with a time step Δt is $\tau_N = 2\Delta t$, corresponding to a maximum frequency, the so-called Nyquist frequency, $\omega_N = \pi/\Delta t$. The sequence $\{f_n\}$ may be regarded as the Fourier coefficients of a function $F(\theta)$:

$$F(\theta) = \sum_{n=-\infty}^{\infty} f_n e^{-in\theta},$$

where $\theta = \omega\Delta t$ is the *digital frequency* and $F(\theta)$ is periodic, $F(\theta) = F(\theta + 2\pi)$. High-frequency components of the sequence may be eliminated by multiplying $F(\theta)$ by a function $H(\theta)$ defined by

$$H(\theta) = \begin{cases} 1, & |\theta| \leq |\theta_c|; \\ 0, & |\theta| > |\theta_c|, \end{cases} \tag{4}$$

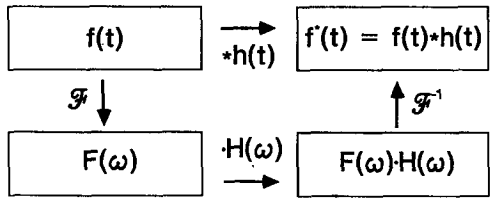

FIG. 1. Schematic representation of the equivalence between convolution and filtering in Fourier space.

where the cutoff frequency $\theta_c = \omega_c\Delta t$ is assumed to fall in the Nyquist range $(-\pi, \pi)$ and $H(\theta)$ has period 2π. This function may be expanded:

$$H(\theta) = \sum_{n=-\infty}^{\infty} h_n e^{-in\theta};$$

$$h_n = \frac{1}{2\pi} \int_{-\pi}^{\pi} H(\theta) e^{in\theta} d\theta. \tag{5}$$

The values of the coefficients h_n follow immediately from (4) and (5):

$$h_n = \frac{\sin n\theta_c}{n\pi}. \tag{6}$$

Let $\{f_n^*\}$ denote the low-frequency part of $\{f_n\}$, from which all components with frequency greater than θ_c have been removed. Clearly,

$$H(\theta) \cdot F(\theta) = \sum_{n=-\infty}^{\infty} f_n^* e^{-in\theta}.$$

The convolution theorem for Fourier series now implies that $H(\theta) \cdot F(\theta)$ is the transform of the convolution of $\{h_n\}$ with $\{f_n\}$:

$$f_n^* = (h*f)_n = \sum_{k=-\infty}^{\infty} h_k f_{n-k}. \tag{7}$$

This enables the filtering to be performed directly on the given sequence $\{f_n\}$. It is the discrete analog of (3). In practice the summation must be truncated at some finite value of k. Thus, an approximation to the low-frequency part of $\{f_n\}$ is given by

$$f_n^* = \sum_{k=-N}^{N} h_k f_{n-k}. \tag{8}$$

As is well known, truncation of a Fourier series gives rise to Gibbs oscillations. These may be greatly reduced by means of an appropriately defined "window" function. The response of the filter is improved if h_n is multiplied by the Lanczos window

$$w_n = \frac{\sin[n\pi/(N+1)]}{n\pi/(N+1)}.$$

The transfer function $T(\theta)$ of a filter is defined as the function by which a pure sinusoidal oscillation is multiplied when subjected to the filter. For symmetric coefficients, $h_k = h_{-k}$, it is real, implying that the phase is not altered by the filter. Then, if $f_n = \exp(in\theta)$, one may write $f_n^* = T(\theta) \cdot f_n$, and $T(\theta)$ is easily calculated by substituting f_n in (8):

$$T(\theta) = \sum_{k=-N}^{N} h_k e^{-ik\theta} = (h_0 + 2\sum_{k=1}^{N} h_k \cos k\theta). \tag{9}$$

The transfer functions for a windowed and unwindowed filter are shown in Fig. 2. These were calculated

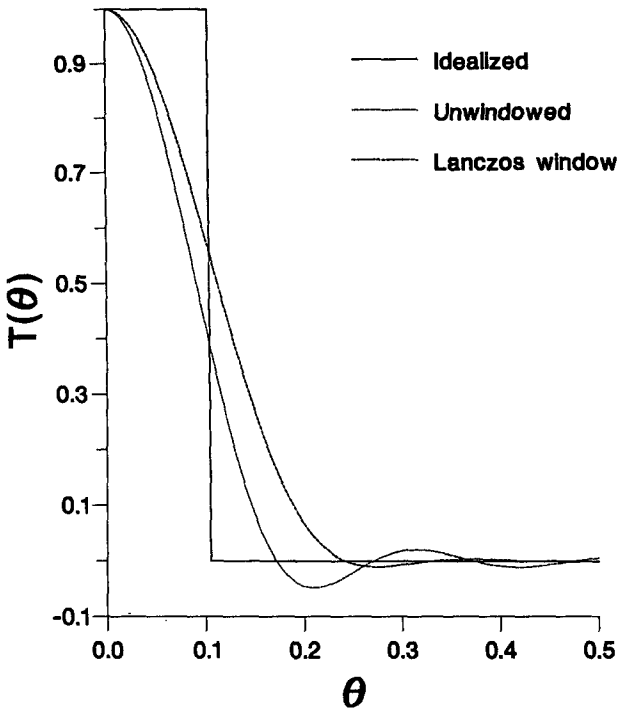

FIG. 2. Transfer functions for the filter defined by the coefficients $h_n = \sin(n\omega_c\Delta t)/n\pi$, where the cutoff period $\tau_c = 2\pi/\omega_c$ is 6 h, with and without modification by a Lanczos window.

for the cutoff period $\tau_c = 6$ h, span $T_s = 2N\Delta t = 6$ h, and time step $\Delta t = 360$ s, as used in section 5. The parameter values are, therefore, $N = 30$ and $\theta_c = \pi/30 \approx 0.1$. It can be seen that the use of the window decreases the Gibbs oscillations in the stop band $|\theta| > |\theta_c|$. However, it also has the effect of widening the pass band beyond the nominal cutoff. For a fuller discussion of windowing see, for example, Hamming (1989).

c. *Digital filters*

Digital signal processing is a crucial aspect of modern communications, and filtering of signals is central to numerous applications of digital electronics. Given a discrete function of time, $\{x_n\}$, a *nonrecursive* digital filter is defined by

$$y_n = \sum_{k=-N}^{N} a_k x_{n-k}. \tag{10}$$

The output y_n at time $n\Delta t$ depends on both past and future values of x_n, but not on other output values. A *recursive* digital filter is defined by

$$y_n = \sum_{k=0}^{N} a_k x_{n-k} + \sum_{k=1}^{M} b_k y_{n-k}. \tag{11}$$

The output y_n at time $n\Delta t$ in this case depends on past and present values of the input, and also on previous output values. Recursive filters are more powerful than nonrecursive ones, but can also be more problematical, as the feedback of the output can give rise to instability. They will not be considered further in this study.

Comparing (8) and (10), it is apparent that the finite approximation to the discrete convolution is formally identical to a nonrecursive digital filter. Thus, the extensive body of theory for such filters can be brought to bear on the present application. This theory is outlined in Hamming (1989), where several methods of designing filters are described. One of the simplest such methods is the expansion of the desired filtering function, $H(\theta)$, as a Fourier series, and the application of a suitable window function to improve the transfer characteristics. That is the method employed in the present case.

3. Application to initialization

a. *Implementation of the filter*

The digital filter defined by (8) was used to process the data provided by an objective analysis scheme, prior to its use as initial data for a forecast using the HIRLAM model. The uninitialized fields of surface pressure, temperature, humidity, and winds were first integrated forward for 3 h, and running sums of the form

$$f_F^*(0) = \tfrac{1}{2} h_0 f_0 + \sum_{n=1}^{N} h_{-n} f_n, \tag{12}$$

where $f_n = f(n\Delta t)$, were calculated for each field at each grid point and on each model level. These were stored at the end of the 3-h forecast. The original fields were then used to make a 3-h "hindcast" during which running sums of the form

$$f_B^*(0) = \tfrac{1}{2} h_0 f_0 + \sum_{n=-1}^{-N} h_{-n} f_n \tag{13}$$

were accumulated for each field and stored as before. The two sums were then combined to form the required summations:

$$f^*(0) = f_F^*(0) + f_B^*(0).$$

These fields correspond to the application of the digital filter (8) to the original data and will be referred to as the filtered data.

The value chosen for the cutoff frequency corresponded to a period $\tau_c = 6$ h. This value was selected on the basis of experiments with a barotropic model (Lynch 1990); a 3-h cutoff yielded similar results, whereas a 12-h cutoff led to damping of the meteorological modes. With the time step $\Delta t = 6$ min used in the model, a 6-h period corresponds to a (digital) cutoff frequency $\theta_c = \pi/30$. The filter coefficients, with a Lanczos window, are given by

$$h_n = \left\{\frac{\sin[n\pi/(N+1)]}{n\pi/(N+1)}\right\}\left[\frac{\sin(n\theta_c)}{n\pi}\right]. \tag{14}$$

The central lobe of the coefficient function spans a period of 6 h, from $t = -3$ h to $t = +3$ h. The summation in (8) was calculated over this range, with the coefficients normalized to have unit sum over the span. Thus, the application of the technique involved computation equivalent to 60 time steps, or a 6-h adiabatic integration.

In order that the backward integration be physically reasonable, all irreversible processes must be disabled. Therefore, both the forward and backward integrations of the model during the filtering procedure were performed with the physics switched off. It is important to emphasize that the filtering is applied to precisely those variables which the model treats in a prognostic manner, namely, temperature, horizontal wind components, humidity, and surface pressure. Moreover, the time-averaging process of the filter is applied at the grid points used by the model, with the same staggering of variables in the horizontal (HIRLAM uses a C grid), and on the model levels (a hybrid vertical coordinate is used, similar to σ at low levels and pressure at high levels). Thus, the filtering does not involve spatial interpolations of any kind and is therefore completely compatible with the discretization of the model.

The values of the variables on the outermost boundary line were held constant during the short-range adiabatic integrations; all values interior to the boundary line were allowed to vary freely. This was done for practical reasons: the boundary data valid for times prior to the initial data time were not available. It would be more consistent with the forecast integration to allow for the temporal variations at the boundaries, and to use the same relaxation scheme as is used for the forecast, and would possibly improve the results. However, as time-dependent boundary conditions normally vary slowly, it is unlikely that such changes would have a significant effect on the initialization. The model integrations normally include a representation of horizontal diffusion. This was also disabled for the integrations to prepare the digitally filtered data.

b. *Relationship between filtering and NMI*

The model equations in normal-mode form may be written

$$\dot{\mathbf{X}} + i\Omega\mathbf{X} + \mathbf{N}(\mathbf{X}) = \mathbf{F}, \tag{15}$$

where $\mathbf{X}$ is the vector of modal amplitudes, Ω is the eigenvalue matrix, $\mathbf{N}$ is a nonlinear vector function, and $\mathbf{F}$ is the diabatic forcing. The modes fall into two categories, low-frequency rotational modes and high-frequency gravity–inertia modes. A cutoff frequency ω_c is chosen to have magnitude lying between these ranges. If the flow is adiabatic and the nonlinear terms are assumed constant in time, the system splits into separate equations:

$$\dot{x}_k + i\omega_k x_k + N_k = 0, \tag{16}$$

one for each mode. For the initial value $x_k(0) = x_k^0$, the solution of (16) is

$$x_k(t) = \left(x_k^0 + \frac{N_k}{i\omega_k}\right)e^{-i\omega_k t} - \left(\frac{N_k}{i\omega_k}\right). \tag{17}$$

Suppose ω_k is a gravity–inertia-mode frequency. The high-frequency part of the solution $x(t)$ can be eliminated by choosing $x_k^0 = -N_k/i\omega_k$. This is the value produced by applying Machenhauer's criterion $\dot{x}_k = 0$ at $t = 0$ to the gravity-wave components, as can be seen from (16). Now consider the result of applying the filtering method: the convolution of $x(t)$ with $h(t) = \sin(\omega_c t)/\pi t$, evaluated at $t = 0$ is

$$(h*x_k)(0) = \begin{cases} x_k^0, & |\omega_k| < |\omega_c|; \\ -N_k/i\omega_k, & |\omega_k| > |\omega_c|. \end{cases} \tag{18}$$

This is precisely the same initial data as for normal-mode initialization.

It is difficult to extend this analysis to the general case described by (15). However, Ballish (1981) has used the simple linear equation

$$\dot{x} + i\omega x + Ne^{-i\nu t} = 0, \tag{19}$$

to compare several initialization schemes. Here ω is a gravity–inertia-wave frequency, ν is a low-frequency characteristic of the synoptic flow, and N is a constant. (Ballish also included an advection term; it is omitted here.) The term $N\exp(-i\nu t)$ mimics the nonlinear forcing of the gravity waves by the rotational modes. The solution of (19) for the initial value $x(0) = x_0$ is

$$x(t) = \left(x_0 - \frac{N}{i\nu - i\omega}\right)e^{-i\omega t} + \left(\frac{N}{i\nu - i\omega}\right)e^{-i\nu t}. \tag{20}$$

Assume that $|\nu| < \omega_c < |\omega|$. Then the convolution of $h(t)$ with the high-frequency term in (20) vanishes, so that at the initial time

$$x_0^* = (h*x)(0) = \left(\frac{N}{i\nu - i\omega}\right).$$

The solution for this initial condition contains only the low-frequency component of (20). Applying Machenhauer's criterion $\dot{x} = 0$ at $t = 0$ gives the initial condition $x(0) = -N/i\omega$; this follows immediately from (19). The solution is then found to be

$$x(t) = -\frac{\nu}{\omega}\left(\frac{N}{i\nu - i\omega}\right)e^{-i\omega t} + \left(\frac{N}{i\nu - i\omega}\right)e^{-i\nu t}. \tag{21}$$

The coefficient of the high-frequency component is small but nonzero. The tendency components due to the two terms are the same size.

The criterion proposed by Machenhauer rests on the assumption that the variation of the nonlinear forcing is slow. The filtering procedure takes the variation of the nonlinear terms into account and should therefore lead to a better balance condition. In the simple case

examined here, the filtering method yielded precisely the initial conditions required for complete removal of the high-frequency oscillations. Ballish (1981) showed that the method formulated by Baer and Tribbia (1977) also has this property. The Machenhauer and Baer–Tribbia initialization techniques are applied by iterative solution of nonlinear equations. In unfavorable circumstances, the iterations may diverge. The convergence properties of a number of initialization schemes have been investigated by Rasch (1985). He used elementary filter theory to deduce the qualitative convergence behavior of the iteration techniques used in these schemes. In the case of the digital filtering scheme developed in this paper, there is no danger of divergence, as the scheme does not involve any iterative process.

4. Forecast model and initial data

a. HIRLAM

HIRLAM is a limited-area primitive equation model with a second-order finite-difference scheme on a staggered C grid and a hybrid sigma-pressure vertical coordinate. This model is comprehensively described in the documentation manual edited by Källberg (1989). The model derived originally from the limited-area version of the ECMWF gridpoint model but has undergone extensive changes during the course of the HIRLAM project. The default version of the model uses a rotated latitude–longitude grid with the North Pole shifted to 30°N, 180° in the mid-Pacific. There is a comprehensive physics parameterization package, for details, see Källberg (1989).

The version of HIRLAM that has been implemented on the CONVEX 220 at MISU was used for all the experiments described in this report. This version includes a consistent scheme for condensation and clouds with cloud water included as a prognostic model variable (Sundqvist et al. 1989). A fourth-order scheme is used for horizontal diffusion. The forecast area is spanned with a grid having 110×100 points with a grid resolution of 0.5° and 16 vertical levels.

The standard normal-mode initialization scheme is described in chapter 3 of the HIRLAM documentation manual (Källberg 1989). It derives from a scheme originally formulated at KNMI (Bijlsma and Hafkenscheid 1986). In the default version of this scheme, all the gravity waves for the first four vertical modes are initialized using adiabatic tendencies and two nonlinear iterations. The humidity field is not changed during the initialization process. The linearization used for the NMI scheme uses a discretization on the mass points of the prediction model. The streamfunction and velocity potential, and thus the vorticity and divergence, are evaluated at these points. The initialization increments are zero at the boundary. The discretization for the NMI scheme is not strictly consistent with the staggered C grid used in the model.

b. The September storm

The analysis of sea level pressure over the model area for 0000 UTC on Thursday, 5 September 1985 is shown in Fig. 3a. The fields produced by the HIRLAM objective analysis, based on observations valid at this time, are taken as the initial data for the forecasts described below. There is a complex low pressure area over and to the west of northern Europe. During the following 24-h period, the low centered over England deepened rapidly and moved eastward to a position over Denmark. Associated with this intense low there were severe winds, reaching 25 m s^{-1} on the Danish west coast, accompanied by heavy precipitation and record early snowfall. Widespread damage occurred as a result of the storm. The sea level pressure analysis for 0000 UTC on Friday, 6 September 1985, is shown in Fig. 3b.

The storm was not particularly well forecast in the numerical predictions available operationally. It was selected as a test case and was investigated exhaustively in a series of experiments during the HIRLAM phase 1 project (Gustafsson et al. 1986). The 24-h forecast of sea level pressure produced by the version of HIRLAM used in the present study is shown in Fig. 3c. It is quite accurate in its prediction of the storm, although the position is slightly too far south and the intensity is marginally overestimated. In a number of experiments (Gustafsson et al. 1986; Sundqvist et al. 1989), the details of the forecast were found to be very sensitive to the precise formulations used for the physical processes.

There are two other features of the synoptic situation shown in Fig. 3 that are worthy of note. The first is a small trough at about 70°N and just west of the prime meridian, which moved southeast during the forecast period, weakening slightly. The second is a large depression near the western boundary of the domain, which deepened and moved approximately northward. The simulation of this depression is critically dependent on information contained in the lateral boundary conditions. The forecast of these two systems in the model run used as a reference (Fig. 3c) was in good agreement with the verifying analysis (Fig. 3b).

Boundary values for the forecasts were obtained from initialized analyses extracted from the ECMWF archives and transformed to the forecast model levels and grid. The values were specified every 6 h and interpolated linearly between these times. The boundary formulation is of the Davies–Källberg type, with a relaxation zone of ten grid points.

5. Results

In this section, the results of applying the digital filtering technique to the initialization of the analysis for HIRLAM will be described. These results will be compared to the results obtained using the normal-mode

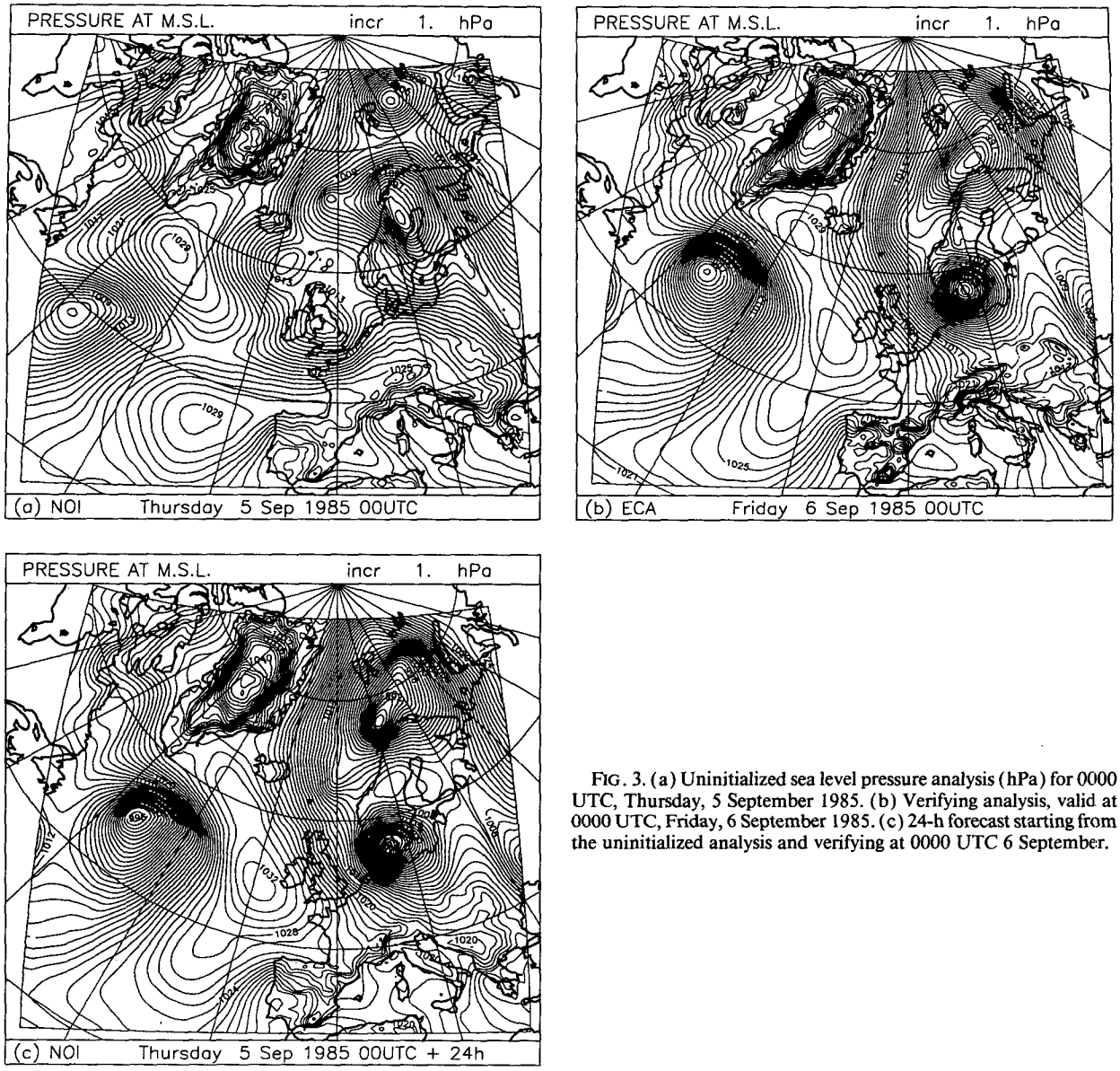

FIG. 3. (a) Uninitialized sea level pressure analysis (hPa) for 0000 UTC, Thursday, 5 September 1985. (b) Verifying analysis, valid at 0000 UTC, Friday, 6 September 1985. (c) 24-h forecast starting from the uninitialized analysis and verifying at 0000 UTC 6 September.

initialization scheme that is the standard method of initialization in HIRLAM. Some initial integrations were carried out adiabatically, that is, with the irreversible physical processes disabled. However, the results described below were for forecasts in which all physical parameterizations were included, as this is the case of primary interest.

For most of the experiments, three parallel model integrations were made: the results will be denoted as follows:

NOI	original analysis (no initialization)
DFI	digital filtering initialization
NMI	normal-mode initialization

Unless otherwise stated, the cutoff period for the digital filtering is 6 h. The humidity is predicted by a conservation equation without evaporation or precipitation processes and is filtered in the same way as the other prognostic fields.

a. Tendency of surface pressure

The primary goal of the initialization is the removal of spurious high-frequency noise from the forecast. A useful global measure of this noise is the mean absolute tendency of surface pressure

$$N_1 = \left(\frac{1}{IJ}\right) \sum_{i=1}^{I} \sum_{j=1}^{J} \left| \frac{\partial p_s}{\partial t} \right|_{ij}.$$

The evolution of this quantity for the three parallel forecasts is depicted in Fig. 4. The severe initial shock resulting from the use of uninitialized data is evident in the graph marked NOI. In this case the mean absolute pressure tendency has an initial value of almost 9 hPa $(3\ \text{h})^{-1}$. It oscillates noisily, decreasing during the forecast due to the damping processes in the model, and reaching an asymptotic value around 1 hPa $(3\ \text{h})^{-1}$ after about 12 h. The normal-mode method reduces the initial value of N_1 to about 2 hPa $(3\ \text{h})^{-1}$, but there is a slight increase during the first few model steps, indicating an imperfection in the degree of balance achieved by the NMI method. The digital filtering results in the lowest values of the noise parameter N_1, which remains roughly constant at about 1 hPa $(3\ \text{h})^{-1}$, corresponding to the asymptotic value for the other runs. Note that the three curves are virtually coincident after 12 h and remain fairly steady thereafter.

In Fig. 5, maps of the initial surface pressure tendency are shown for the three forecasts. The uninitialized run (Fig. 5a) has some extremely large values. The highest values occur over the European area, but it should be noted that values in excess of 20 hPa $(3\ \text{h})^{-1}$ occur over the ocean. Figure 5b is for the data after digital filtering. Note that the contour interval is now reduced by a factor of 10. The reduction in the values of initial tendency are dramatic; the spatial scale of the tendency field is larger than before and appears to be synoptically reasonable. For example, the falling pressure east of England and the large area of rising pressure in the Atlantic are easily related to pressure systems in the analysis and to pressure changes that occurred during the period of the forecast. Figure 5c is for the data after NMI. The values of initial tendency are again very much smaller than in the uninitialized case, but the reduction is not as great as for the filtering. A considerable amount of noise still remains, most pronounced in regions where there are steep orographic slopes. Thus, the tendency values in the alpine region are large, whereas those over the Greenland plateau are relatively small. In general, the patterns of pressure change bear little relationship to the synoptic flow and are smaller in spatial scale.

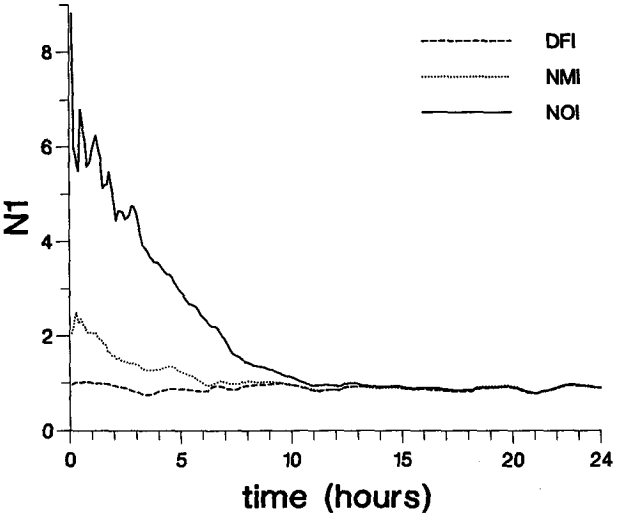

FIG. 4. Mean absolute surface pressure tendency N_1 [hPa $(3\ \text{h})^{-1}$] averaged over the forecast area. The curves for the three forecasts are shown: NOI is the forecast without initialization; DFI is for the data after digital filtering; NMI is for the normal-mode initialized analysis.

The surface pressure forecast for the first 6 h of the three runs at two model grid points may be seen in Fig. 6. The first point (at $I = 81$, $J = 23$) is over the Alps and the second (at $I = 30$, $J = 30$) is in the mid-Atlantic. The noisy character of the uninitialized forecast is abundantly clear, particularly at the mountain point, where the tendency values during the initial hours are completely unrealistic. This noise is reduced for the initialized runs; however, there is still a residue of high-frequency noise in the NMI forecast; the digitally filtered run is considerably less noisy.

b. *Changes in the initial fields*

A requirement of any initialization procedure is that the changes made in the initial data be acceptably small. In general, they should be similar in size or smaller than the expected analysis error to ensure that the analysis is not degraded by the initialization process. Table 1 contains the root-mean-square (rms) and maximum changes made to the initial fields of surface pressure, temperature, and wind components by the DFI and NMI schemes. The changes are reasonable in magnitude, generally less than the size of the observational error. The maximum changes are somewhat larger for the digital filtering scheme; the root-mean-square changes are very similar for DFI and NMI.

The sea level pressure maps for DFI and NMI are shown in Figs. 7a and 7b. To the eye, they are very similar to each other and also to the original pressure analysis (Fig. 3a); indeed, it is hard to detect any differences between the three maps. The uninitialized pressure was subtracted from each of these fields to obtain charts of the changes in pressure induced by DFI and NMI; however, these have not been reproduced, as they did not contain any features of note.

c. *Changes in the forecasts*

In addition to the requirement that the changes made in the initial data be acceptably small, it is reasonable to expect that a forecast from initialized data should closely resemble the uninitialized forecast. In fact, for a model incorporating damping processes that attenuate the gravity–inertia components of the flow, the two forecasts should tend to converge, at least on a time scale of a day or so. Thus, the differences between the 24-h forecasts with and without initialization should be smaller than the changes made by the initialization.

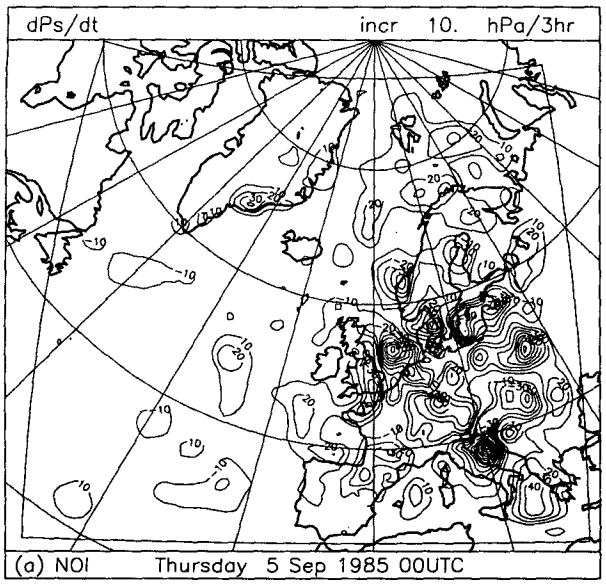

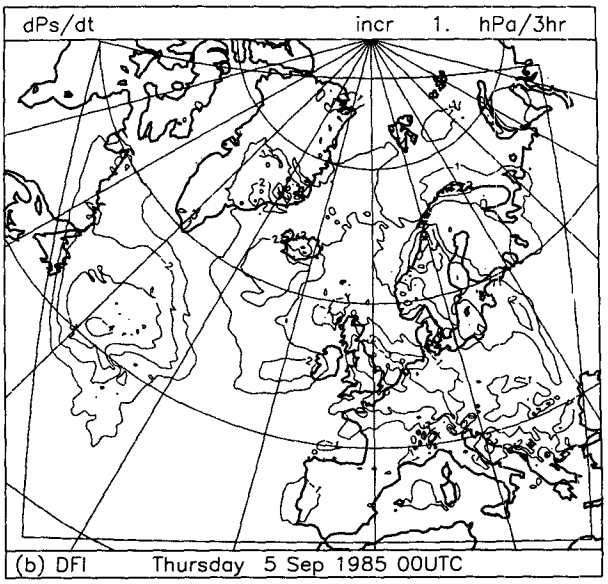

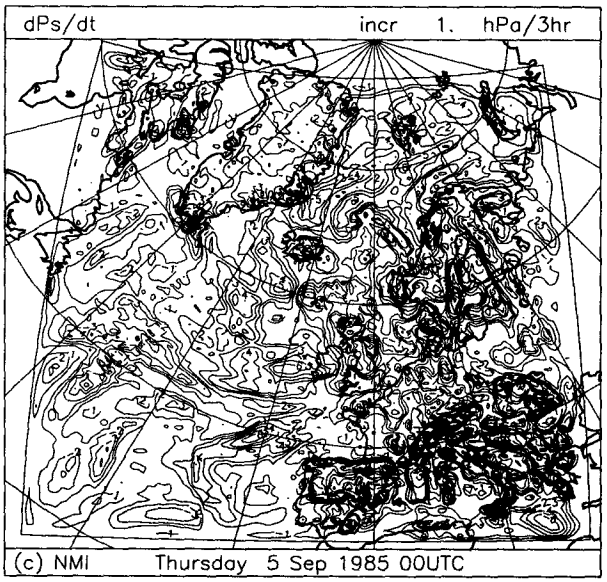

FIG. 5. Initial surface pressure tendency [hPa ($3\ h^{-1}$)] for the three initial datasets: (a) NOI, (b) DFI, and (c) NMI. [Note: contour interval ten-times greater for the uninitialized case (a); positive contours solid, negative contours dashed, zero contour suppressed.]

Table 2 contains the rms and maximum differences in surface pressure, temperature, and wind components between the forecasts starting from the two initialized datasets and the uninitialized forecast. Comparing the values with those in Table 1, the rms differences are seen to have decreased markedly; they are very similar for DFI and NMI. The maximum wind differences are somewhat larger, while the maximum pressure difference is slightly smaller for DFI than for NMI.

The DFI and NMI forecasts of sea level pressure are shown in Figs. 8a and 8b. The two maps are virtually identical to each other and also practically indistinguishable from the reference forecast (Fig. 3c). The difference maps (not plotted) confirmed that there is no significant difference between the three forecasts. The rms difference of 0.07 hPa, the same for both initialized forecasts, is remarkably small.

There is essentially no difference between the three forecasts of the intensity and position of the September storm. This is the feature of most interest in the forecast charts, and any such difference might be significant in an operational context. The convergence between the uninitialized and initialized runs is reassuring. The precise position of the storm center is in error in all forecasts, and the depth of the depression is exaggerated. The storm has been simulated many times with numerous model variations (see, for example, Gustafsson et al. 1986), and the forecast position was found to be quite sensitive to the details of the physical parameterizations.

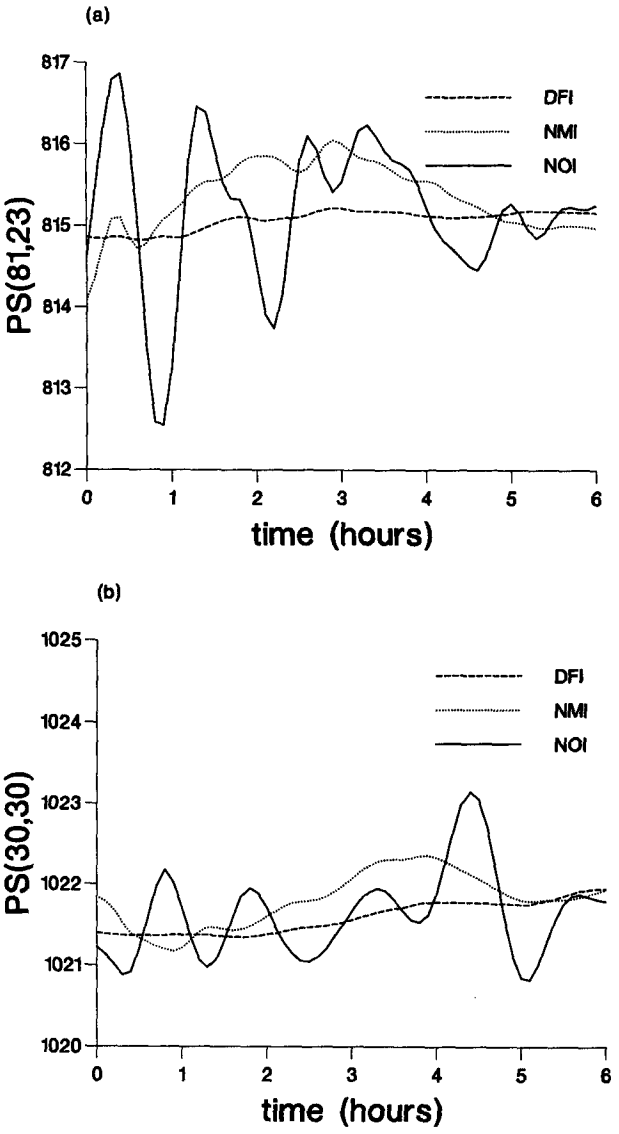

FIG. 6. Surface pressure variation (hPa) for the first 6 h, at two model grid points, for the forecasts from the three initial states, NOI, DFI, and NMI. (a) Point $I = 81$, $J = 23$, in the Alps and (b) point $I = 30$, $J = 30$, in the mid-Atlantic.

Claims have occasionally been made in the literature about the ability of initialization to improve forecast accuracy; however, such claims must be viewed with considerable suspicion. The justification for modifying the gravity–inertia components of the analysis is that their effect on the rotational flow is weak; thus, they may be altered to remove noise without greatly influencing the ensuing forecast. Williamson and Temperton (1981) compared the effects of applying an initialization before the forecast and to the final fields and found that very similar results were obtained; that is, there was little difference between the imposition of balance before and after the time integration. In the present case, the diffusive processes and boundary relaxation scheme ensure the eventual removal of gravity–inertia-wave noise and lead to a coalescence between the three forecasts. The close similarity between the initialized and uninitialized runs is comforting: the initialization schemes are behaving in precisely the intended fashion, in removing the noise without affecting the forecast.

d. Precipitation forecasts

The precipitation rate (mm day^{-1}) is plotted in Fig. 9. This is the value averaged over the forecast area. The rainfall rate increases steadily during the forecast period. This is perhaps reasonable in view of the intensification of both the September storm and the Atlantic depression, but it should be recalled that underprediction of rainfall during the first few forecast hours is a common feature of primitive equation models. There is essentially no difference between the NOI, DFI, and NMI graphs. The total precipitation accumulated during the 24 h is plotted in Fig. 10 for the NOI forecast (the DFI and NMI results are not plotted as they are so similar to the case shown). Quantitative verification of rainfall forecasts is problematical; however, the pattern of precipitation is in harmony with the synoptic situation. The consequences of initialization for precipitation forecasts will be investigated in a subsequent study in which diabatic effects will be incorporated into the DFI scheme.

e. Further consideration of noise

The surface pressure tendency is an excellent *barometer* of the noise in a forecast, but it provides only a limited view. The change in surface pressure is determined by the vertically integrated convergence of mass above the point in question. It is possible, and indeed usual in the atmosphere, for the pressure tendency to be small as a result of cancellations between relatively large values of convergence and divergence at different levels. This compensation effect has long been observed empirically in diagnostic studies. It was considered by Platzman (1967) in his discussion of Richardson's forecast. It is of interest to examine it in the present context.

TABLE 1. Root-mean-square (rms) and maximum (max) differences in temperature, wind components, and surface pressure between the initialized and uninitialized analysis. (DFI − NOI): changes due to digital filtering; (NMI − NOI): changes due to normal-mode initialization.

	T (K)		u (m s^{-1})		v (m s^{-1})		p_s (hPa)	
	rms	max	rms	max	rms	max	rms	max
DFI − NOI	0.11	1.38	0.40	4.24	0.43	5.28	0.37	1.61
NMI − NOI	0.11	0.98	0.39	3.19	0.44	3.99	0.32	1.29

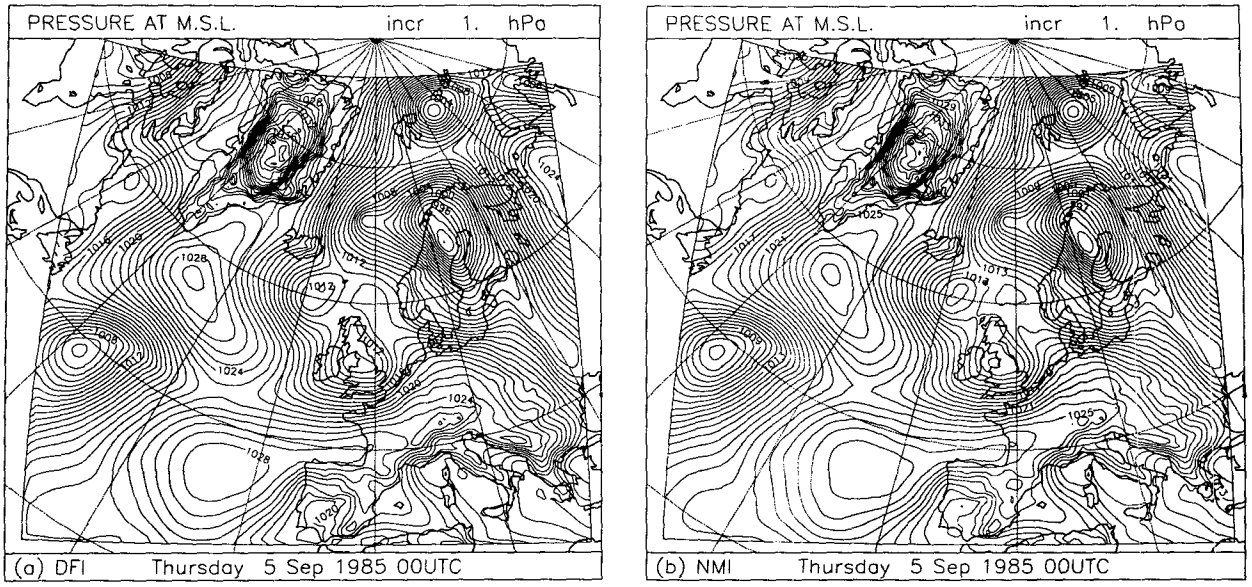

FIG. 7. (a) Sea level pressure analysis (hPa) for 0000 UTC, Thursday, 5 September 1985 after digital filtering (DFI). (b) Corresponding analysis, valid after normal-mode initialization (NMI).

The vertically integrated continuity equation (in hybrid η coordinates) yields the surface pressure tendency equation

$$\frac{\partial p_s}{\partial t} = -\int_0^1 \nabla\cdot\left(\mathbf{V}\frac{\partial p}{\partial \eta}\right)d\eta.$$

The vertical compensation effect is related to the fact that

$$\left|\int_0^1 \nabla\cdot\left(\mathbf{V}\frac{\partial p}{\partial \eta}\right)d\eta\right| \leq \int_0^1\left|\nabla\cdot\left(\mathbf{V}\frac{\partial p}{\partial \eta}\right)\right|d\eta.$$

In general, random cancellations will ensure that the left-hand side of this inequality is substantially less than the right-hand side, but it is the more systematic cancellations between convergence and divergence that are of interest here. With a discrete vertical coordinate, the mean absolute pressure tendency is given by

$$N_1 = \left(\frac{1}{IJ}\right)\sum_{i=1}^{I}\sum_{j=1}^{J}\left|\sum_{k=1}^{K}(\nabla\cdot\Delta p_k\mathbf{V}_k)_{ij}\right|.$$

To determine the extent to which the compensation effect plays a role in the analyses under consideration, the mean absolute mass divergence

$$N_2 = \left(\frac{1}{IJ}\right)\sum_{i=1}^{I}\sum_{j=1}^{J}\sum_{k=1}^{K}|\nabla\cdot\Delta p_k\mathbf{V}_k|_{ij}$$

was computed each time step for the three forecasts. The compensation effect may be evaluated by defining a *balance ratio*

$$\mathrm{Br} = \frac{100N_1}{N_2}.$$

The factor of 100 conveniently allows Br to be expressed as a percentage of its maximum possible value. The smaller it is, the more significant is the compensation effect.

The evolution of N_2 is plotted in Fig. 11a. For the NMI analysis, the initial value is hardly changed; in the case of DFI, it is reduced by about 15%. In all cases N_2 decreases over the first 6 h or so, suggesting that the initial values are too high. There is an interesting feature visible in all the graphs: the quantity N_2 has peaks every 6 h, corresponding to the intervals when the boundary fields are specified. Clearly, the discontinuities in the time derivatives of the boundary data associated with linear interpolation of these values in time are resulting in some noise in the forecasts, though this effect appears not to be too severe.

The balance ratio Br is plotted in Fig. 11b. For the NOI case its initial value is relatively high (7%), demonstrating that compensation between convergence and divergence is far from complete in the uninitialized analysis. For NMI, the initial value of Br has fallen to 2%, indicating that this initialization procedure has re-

TABLE 2. Root-mean-square (rms) and maximum (max) differences in temperature, wind components, and surface pressure between the forecasts starting from the two initialized datasets and the uninitialized forecast. (DFI − NOI): changes due to digital filtering; (NMI − NOI): differences due to normal-mode initialization.

	T (K)		u (m s^{-1})		v (m s^{-1})		p_s (hPa)	
	rms	max	rms	max	rms	max	rms	max
DFI − NOI	0.07	2.21	0.18	6.24	0.18	5.70	0.07	1.31
NMI − NOI	0.06	1.91	0.17	2.14	0.19	3.26	0.07	1.94

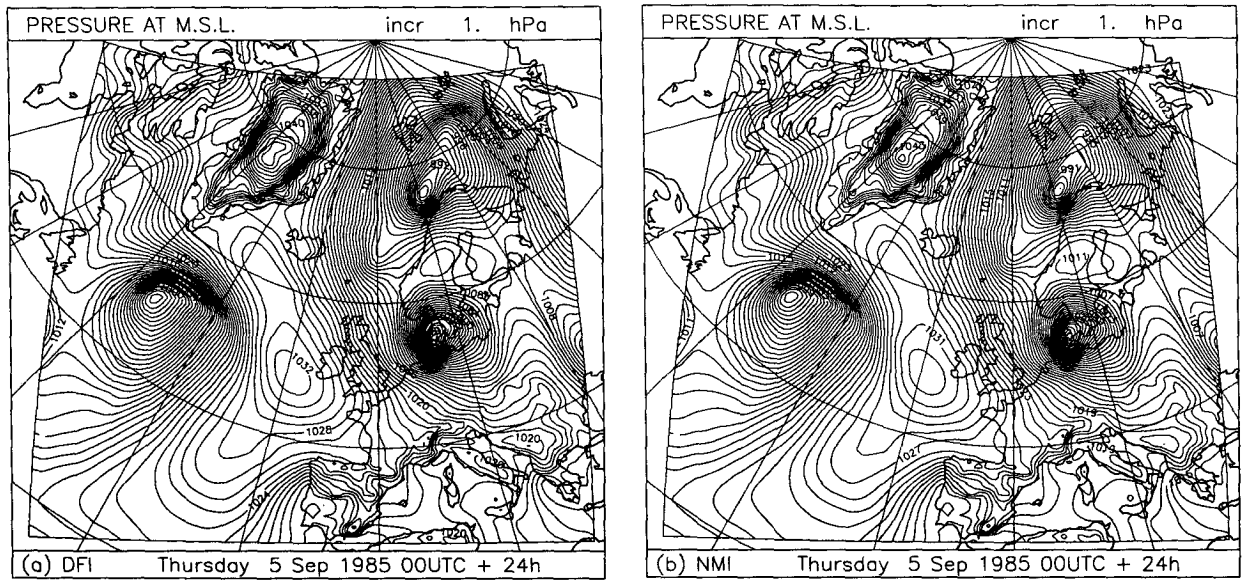

FIG. 8. (a) 24-h forecast sea level pressure (hPa) starting from the DFI data. (b) 24-h forecast sea level pressure starting from the NMI data.

sulted in an establishment of greater compensation between convergence and divergence. For the digitally filtered analysis the value of Br is lower still, and the ratio remains more or less steady at the asymptotic value of about 1%.

The compensation effect at two particular model grid points was also examined. The points chosen were again $I = 81$, $J = 23$ in the Alps and $I = 30$, $J = 30$ in the mid-Atlantic. The mass divergence $m_k = \nabla \cdot (\Delta p_k \mathbf{V}_k)$ at each model level is given in Table 3. The absolute value of the sum of m_k over all levels yields the magnitude of the pressure tendency

$$n_1 = \left| \sum_{k=1}^{K} m_k \right| = \left| \frac{\partial p_s}{\partial t} \right|$$

at the grid point. This is compared to the sum n_2 of the magnitudes of m_k, to obtain a local measure of the balance:

$$n_2 = \sum_{k=1}^{K} |m_k|; \quad \text{br} = \frac{100 n_1}{n_2}.$$

The values of these quantities are given in Table 3. There appears to be a high degree of random cancellation between the levels: the ratio br is nowhere higher than 12%. The quantities n_1, n_2, and br are comparable in size for the uninitialized data (NOI) and normal-mode initialized (NMI) analyses. For the digitally filtered data the mean absolute mass divergence n_2 is decreased to a greater extent, and the reduction in the magnitude of the pressure tendency is dramatic, even at the mountain point. The enhancement of the compensation effect is spectacular, the local balance ratio being only a fraction of a percent.

f. The diagnostic fields

In Fig. 12, the vertical velocity $\omega = dp/dt$ at 500 hPa and at grid points (81, 23) and (30, 30), for the first 6 h of the three forecasts, shows that the spurious oscillations in the uninitialized run are, to great extent, removed by initialization. The filtering appears to be more effective than the normal-mode initialization in suppressing them. The vertical velocity at 500 hPa at the initial time was plotted for the three analyses (not shown). The initialized fields were much smoother than the original analysis, but still contained many

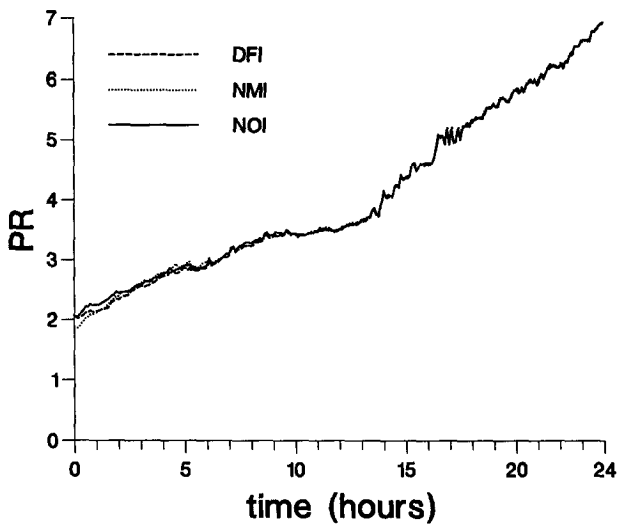

FIG. 9. Precipitation rate (mm day^{-1}) vs time for the three forecasts averaged over the forecast area.

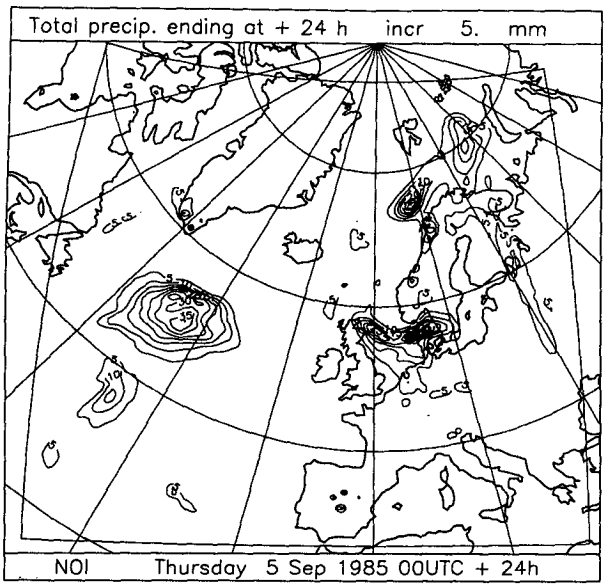

FIG. 10. Total accumulated precipitation (mm) for the 24-h period, predicted by the forecast from the uninitialized analysis NOI.

subsynoptic-scale features. The fields after 24 h were very similar for the three forecasts, and the features of the vertical velocity field were clearly correlated with the synoptic flow.

The rms divergence at each model level, for the three analyses, is plotted in Fig. 13. The normal-mode initialization does not bring about a significant change in this quantity, except at the uppermost level. The filtering reduces it by a more or less constant amount of about 2×10^{-6} s^{-1} at each level. The initial divergence fields after DFI and NMI, at the lowest and highest model levels, were plotted (not shown). The fields at the lowest level appeared very similar; at the upper level the DFI field was much smoother, but the values at that level are relatively small, so this may not have too much significance.

There is some evidence that gravity waves may provide a triggering mechanism for the development of severe storms. In such a case it may be argued that damping of these modes by an initialization scheme may suppress the development of significant meteorological features. In view of the close similarity between the forecasts previously discussed, this does not appear to be a problem in the present context.

6. Discussion

a. Background

The idea of filtering in time goes right back to Richardson (1922). In analyzing the likely cause of the "glaring error" in his forecast, Richardson focused on errors in the initial winds that resulted in unrealistic values of the divergence. He proposed several methods of smoothing the data to alleviate the problem, one such method being to take the average value of observations made at successive times. The method described in this paper uses a similar idea, but the time series are generated by the model rather than by repeated observations and the time filter is designed for improved selectivity.

A method of filtering in time to remove high-frequency noise has been applied operationally at the Deutscher Wetterdienst for many years (Edelmann

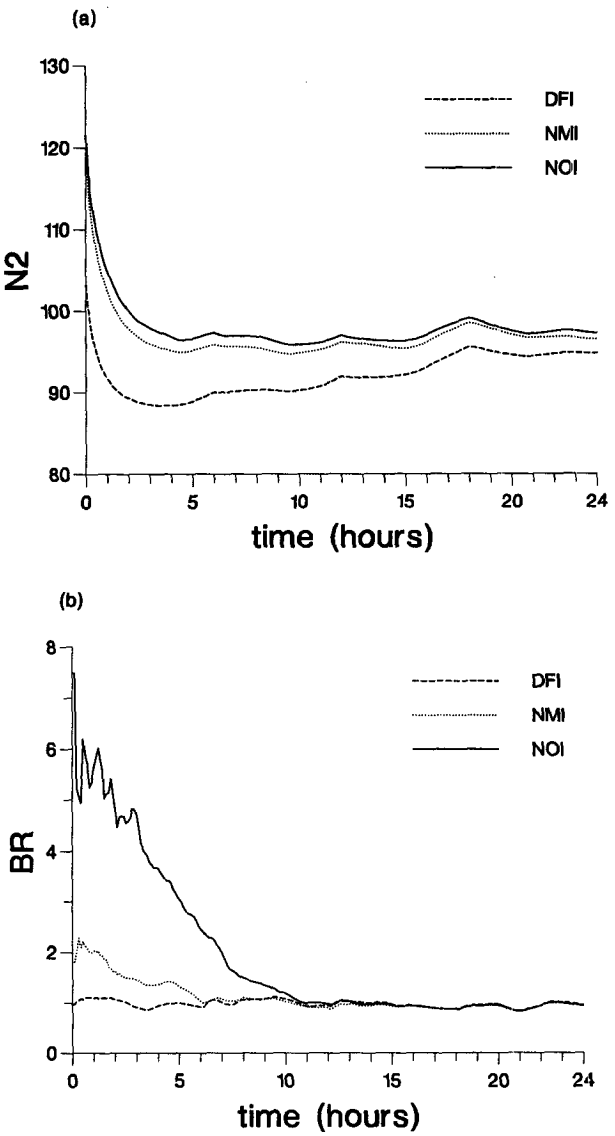

FIG. 11. (a) Mean absolute mass divergence N_2 [hPa (3 h)$^{-1}$] and (b) balance ratio (Br = $100N_1/N_2$) for the three forecasts. NOI: without initialization; DFI with digital filtering; NMI with normal-mode initialization.

TABLE 3. Mass divergence at each model level, at grid points $I = 30$, $J = 30$ (ocean) and $I = 81$, $J = 23$ (mountain) for the three analyses. Here n_1 is the magnitude of the vertical sum, n_2 is the vertical sum of the magnitudes, and br = $100n_1/n_2$ is the local balance ratio.

	Ocean point			Mountain point		
k	NOI	DFI	NMI	NOI	DFI	NMI
1	−2.07	−0.64	−0.30	1.82	0.18	1.82
2	4.15	1.68	0.81	−6.69	−5.60	−5.74
3	−1.09	0.78	−1.93	23.65	20.51	22.78
4	11.75	5.24	13.12	2.15	2.29	0.07
5	−17.53	−14.96	−15.89	−30.71	−20.32	−31.90
6	−19.30	−9.13	−18.08	16.34	7.67	15.47
7	15.75	11.57	16.55	−27.46	−18.46	−27.86
8	−0.70	0.44	−0.42	9.10	15.00	8.87
9	1.89	−0.27	1.84	28.71	24.02	28.41
10	2.54	−0.16	2.22	31.01	19.93	30.67
11	−2.68	1.34	−3.49	3.41	−5.82	2.84
12	2.45	3.63	1.97	1.90	−3.31	1.45
13	−6.05	−5.87	−6.23	−0.40	−3.58	−0.61
14	1.00	0.30	0.51	−8.72	−12.09	−8.88
15	6.26	4.85	5.86	−14.14	−15.62	−14.50
16	−0.12	0.77	0.26	−4.99	−5.42	−4.81
n_1 =	3.73	0.42	3.19	24.97	0.61	18.07
n_2 =	95.31	61.64	89.49	211.19	179.83	206.69
br =	3.91	0.68	3.56	11.82	0.34	8.74

1972). The model is integrated forward for 6 h, time averages of the variables are computed and assumed to be applicable 3 h after the analysis time and the integration proceeds from there. The method reduces high-frequency oscillations in the ensuing forecast. Its effectiveness would be enhanced by an adjustment of the filter weights to obtain a sharper discrimination between low and high frequencies.

The digital filtering technique has been used to initialize data for a limited-area shallow-water model (Lynch 1990). Since that model had a semi-Lagrangian formulation of advection, a time step of 45 min could be used. Thus, only three steps forward and three backward were required to apply a filter with a span of 6 h (the weights vanish at $t = \pm 3$ h, so the variables are not needed at these times). The method was successful in eliminating gravity–inertia oscillations from the forecast. Another application of the technique was made to initialize the idealized data used by Richardson for the "introductory example" in chapter 2 of his book (Lynch 1992). It was shown there that the cutoff frequency could be selected to preserve the Kelvin wave while eliminating higher-frequency gravity waves.

b. *Advantages of digital filtering*

The outstanding characteristic of the digital filtering technique is its great simplicity, both in the underlying ideas and in their practical implementation. An initialization scheme for an existing model can be developed in a matter of hours using the DFI method. This contrasts sharply with the very considerable investment of effort required to implement an NMI scheme. Yet, the filtering technique has been shown to be at least as effective as the normal-mode method.

The results discussed in section 5 suggested that the DFI method was superior to NMI in suppressing high-frequency noise. However, it is only fair to point out that there is scope for improving the performance of

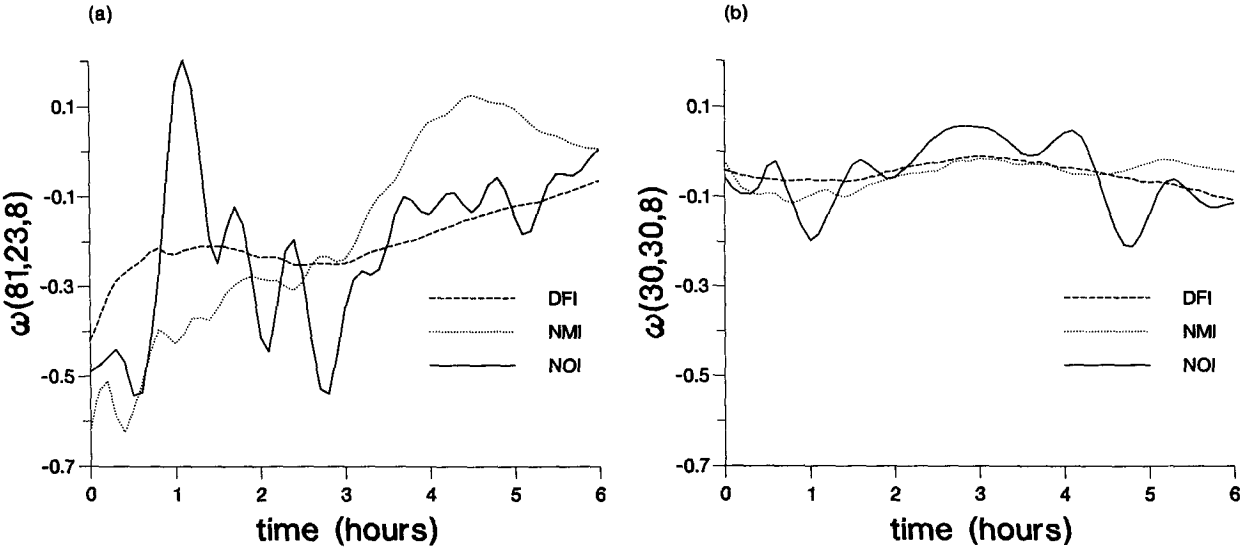

FIG. 12. Vertical velocity $\omega = dp/dt$ (Pa s^{-1}, at 500 hPa, at two model grid points for the three forecasts: (a) Point $I = 81$, $J = 23$, in the Alps, and (b) point $I = 30$, $J = 30$, in the mid-Atlantic.

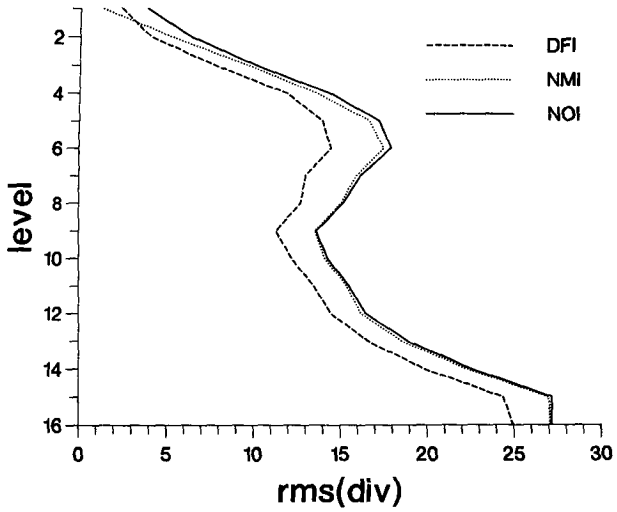

FIG. 13. Root-mean-square divergence (10^{-6} s^{-1}) at each model level, for the uninitialized analysis (NOI), the digitally filtered analysis (DFI), and the normal-mode initialized analysis (NMI).

the normal-mode scheme and for increasing its compatibility with the forecast model. It is likely that if such changes were made, the efficacy of the NMI scheme would equal that of DFI. The primary advantage of the digital filtering technique is the ease with which it can be implemented.

The DFI technique can be applied without knowledge of the model normal modes. This is especially useful for limited-area models, or global models using other than standard geographical coordinates, in which case the horizontal variables cannot be separated and extraction of normal modes requires simplifying assumptions. If normal modes are calculated each time NMI is employed, the computation becomes prohibitive; on the other hand, storage requirements to retain them are not inconsiderable and increase rapidly with the number of degrees of freedom of the model. These difficulties will be aggravated for nonhydrostatic models, which have a richer spectrum of eigenmodes.

The separation of the fields into vertical modes is undertaken as a part of the process of NMI, and also in the case of implicit formulations of the normal-mode technique (Bourke and McGregor 1983; Temperton 1988). A modified geopotential, depending on temperature and surface pressure, is introduced to cast the equations for each vertical mode in shallow-water form. The partitioning of changes in the modified variable into changes in temperature and surface pressure is to some extent arbitrary. Since the DFI scheme applies directly to the model prognostic variables, such an ambiguity never arises.

The digital filtering uses values produced by the forecast model, with precisely the same horizontal discretization and vertical levels used for the forecast. Thus, complete compatibility between the initialization and forecast is assured. Any changes to the model formulation automatically apply to the filtering process, which may easily be incorporated into the model code, obviating the need for additional maintenance of the initialization system; this is a significant practical advantage.

The computation time required to apply the digital filtering scheme was 554 s. Almost all of this was spent making the forward and backward integrations, which covered a total span of 6 h. The time required for the normal-mode initialization was 455 s with two nonlinear iterations of four vertical modes. Much of this time is spent solving Poisson equations to extract wind changes from the streamfunction and velocity potential. This time does not include the calculation of the eigenmodes; if these need to be calculated, the total time for the NMI scheme is more than doubled, to 1149 s.

An application of the filtering scheme with the same cutoff period (6 h) but with the span $T_s = 2N\Delta t$ reduced to 3 h (i.e., forward and backward integrations of 1.5 h) was tried. The noise profile of the quantity N_1 for this case is plotted in Fig. 14, along with the previous results for the DFI and NMI analyses. The reduction of noise is not quite as effective as with a 6-h span, but is still greater than that obtained using normal-mode initialization. Since the computation time is proportional to the span, a 50% reduction is achieved by means of this change, and the results may well be adequate for operational application of the technique. It is evident that there is a potential for further improvement by a more careful design of the digital filter.

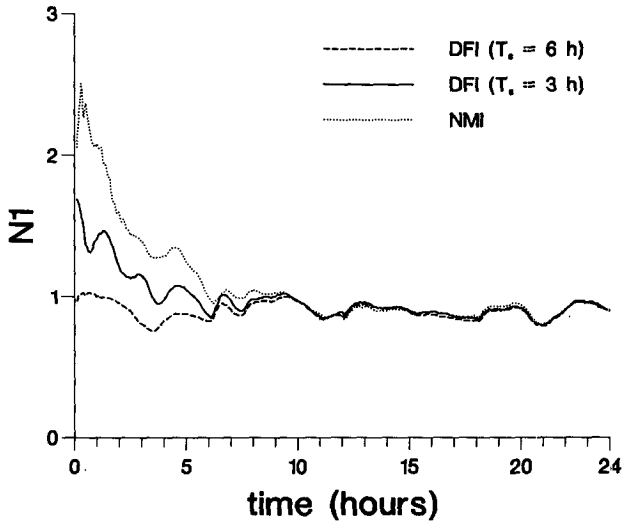

FIG. 14. Mean absolute surface pressure tendency N_1 [hPa (3 h)$^{-1}$] averaged over the forecast area. Dashed: digitally filtered analysis (τ_c = 6 h, T_s = 6 h); solid: digitally filtered analysis (τ_c = 6 h, T_s = 3 h); dotted: normal-mode initialized analysis.

c. Diabatic initialization

The filtering scheme used in this study was applied to time series generated by an adiabatic integration. A suggested method for inclusion of irreversible diabatic processes will now be described. Let the analyzed value of a particular variable at a particular model grid point be Φ_a. The model is integrated backward for a time $T/2$, where T is the filter span, without the irreversible physics, that is, adiabatically. A diabatic forecast of length T is now made from $t = -T/2$ to $t = +T/2$, producing a time series for Φ denoted by $\Phi_d(t)$. The value of $\Phi_d(0)$ will, in general, differ from the analyzed value Φ_a. Now the filter is applied to $\Phi_d(t)$, yielding a value Φ_d^*. If the original analysis were $\Phi_d(0)$, then Φ_d^* would be the appropriate filtered data. However, since this is not the case, Φ_d^* is adjusted to allow for the difference by the following definition of the filtered fields:

$$\Phi^* \equiv \Phi_d^* - [\Phi_d(0) - \Phi_a].$$

In the case where there is no difference between Φ_a and $\Phi_d(0)$, this method gives the filtered value for a series of model states evolving diabatically and passing through the analyzed value at the initial time. Preliminary studies using this method for incorporating diabatic effects have yielded promising results and will be reported in a future publication. Finally, it is observed that Fox-Rabinowitz and Gross (1990) report the removal of the initial spinup effect by means of a 3-h backward adiabatic integration followed by a 3-h forward diabatic forecast, using a damping integration scheme.

d. Further remarks

The design of the filter used in this study used only the most basic ideas of filter theory and one of the simplest windows. Many more sophisticated techniques for optimizing filter performance have been developed in the context of digital signal processing (see, e.g., Hamming 1989 and references therein). These could be employed to design a filter based on objective criteria, and to ensure maximum effectiveness for a given computational cost. The resources devoted to filter design need be expended only once, but yield benefits that are reaped repeatedly.

The DFI scheme formulated in this paper does not involve constraints on the mass or wind fields. It would be straightforward to devise a DFI scheme in which one or other of these fields was constrained to be constant, in a manner similar to that of constrained initialization based on the normal-mode method. Such a scheme would involve an iterative process, with consequent increase in computational expense. Therefore, it would be preferable to develop a constrained scheme using the more efficient filters alluded to previously.

A final remark concerns the use of recursive filters. In the context of initialization nonrecursive filtering seems most natural. However, it seems reasonable that filtering integration schemes can be developed using the digital filtering technique, and in that context the recursive filter should be more useful. Filtering integration schemes have been developed by Lynch (1991), using Laplace and Z transforms. If such schemes were formulated directly in the physical domain, using digital filtering techniques, they would be computationally more economical and might be applicable in the field of data assimilation.

Acknowledgments. The authors would like to thank Per Kållberg for providing analyzed fields and Nils Gustafsson for assistance in implementing the NMI scheme. The figures were produced with the "MetgraF" Package developed at SMHI. Peter Lynch wishes to express his gratitude to Erland Källén for the opportunity to spend two months as a visiting scientist at the International Meteorological Institute in Stockholm. Xiang-Yu Huang is supported by NFR (Swedish National Science Research Council) Contracts E-EG 2923-300 and G-GU 1705-311.

REFERENCES

Baer, F., and J. Tribbia, 1977: On complete filtering of gravity modes through nonlinear initialization. *Mon. Wea. Rev.*, **105,** 1536–1539.

Ballish, B. A., 1981: A simple test of the initialization of gravity modes. *Mon. Wea. Rev.*, **109,** 1318–1321.

Bijlsma, S. J., and L. M. Hafkenscheid, 1986: Initialization of a limited area model: A comparison between the nonlinear normal mode and bounded derivative methods. *Mon. Wea. Rev.*, **114,** 1445–1455.

Båth, Markus, 1974: *Spectral Analysis in Geophysics.* Elsevier Scientific Publishing Company, 563 pp.

Bourke, W., and J. L. McGregor, 1983: A nonlinear vertical mode initialization scheme for a limited area prediction model. *Mon. Wea. Rev.*, **111,** 2285–2297.

Edelmann, W., 1972: Initial balancing and damping of gravity oscillations for forecast models including the orography. *Beitr. Atmos. Phys.*, **45,** 94–120.

Fox-Rabinovitz, M. S., and B. D. Gross, 1990: The removal of initial spin-up effect by diabatic initialization in the GLA data assimilation system. In *Research Activities in Atmospheric and Ocean Modelling,* CAS/JSC Working Group on Numerical Experimentation. Report No. 14, WMO Secretariat, Geneva. p. 1.13.

Gustafsson, N., S. Järvenoja, P. Kållberg, and N. Woetmann Nielsen, 1986: Baseline experiments with a high resolution limited area model. HIRLAM Technical Report No. 1, 87 pp. [Available from SMHI, S 60176 Norrköping, Sweden.]

Kållberg, P., Ed., 1989: The HIRLAM level 1 system. Documentation manual, 160 pp. [Available from SMHI, S 60176 Norrköping, Sweden.]

Lynch, Peter, 1990: Initialization using a digital filter. In *Research Activities in Atmospheric and Ocean Modelling,* CAS/JSC Working Group on Numerical Experimentation. Report No. 14, WMO Secretariat, Geneva. 1.5–1.6.

——, 1991: Filtering integration schemes based on the Laplace and Z transforms. *Mon. Wea. Rev.*, **119,** 653–666.

——, 1992: Richardson's barotropic forecast: A reappraisal. *Bull. Amer. Meteor. Soc.*, **73,** 35–47.

Hamming, R. W., 1989: *Digital Filters.* Prentice-Hall International, 284 pp.

Machenhauer, B., 1977: On the dynamics of gravity oscillations in a shallow water model with applications to normal mode initialization. *Beitr. Atmos. Phys.*, **50,** 253–271.

Platzman, G. W., 1967: A retrospective view of Richardson's book on weather prediction. *Bull. Amer. Meteor. Soc.*, **48,** 514–550.

Rasch, P. J., 1985: Developments in normal mode initialization. Part 1: A simple interpretation for normal mode initialization. *Mon. Wea. Rev.*, **113,** 1746–1752.

Richardson, L. F., 1922: Weather Prediction by Numerical Process. Cambridge Univ. Press, 236 pp. Reprinted by Dover Publications, New York, 1965.

Sundqvist, H., E. Berge, and J. E. Kristjánsson, 1989: Condensation and cloud parameterization studies with a mesoscale numerical weather prediction model. *Mon. Wea. Rev.*, **117,** 1641–1657.

Temperton, C., 1988: Implicit normal mode initialization. *Mon. Wea. Rev.*, **116,** 1013–1031.

——, and D. L. Williamson, 1981: Normal mode initialization for a multilevel gridpoint model. Part 1: Linear aspects. *Mon. Wea. Rev.*, **109,** 729–743.

Williamson, D. L., and C. Temperton, 1981: Normal mode initialization for a multi-level gridpoint model. Part 2: Nonlinear aspects. *Mon. Wea. Rev.*, **109,** 744–757.